JCI insight

The DNA repair protein ATM as target in autism spectrum disorder

Lara Pizzamiglio, … , Elisabetta Menna, Flavia Antonucci

JCI Insight. 2020. https://doi.org/10.1172/jci.insight.133654.

Research In-Press Preview Development Neuroscience

Graphical abstract

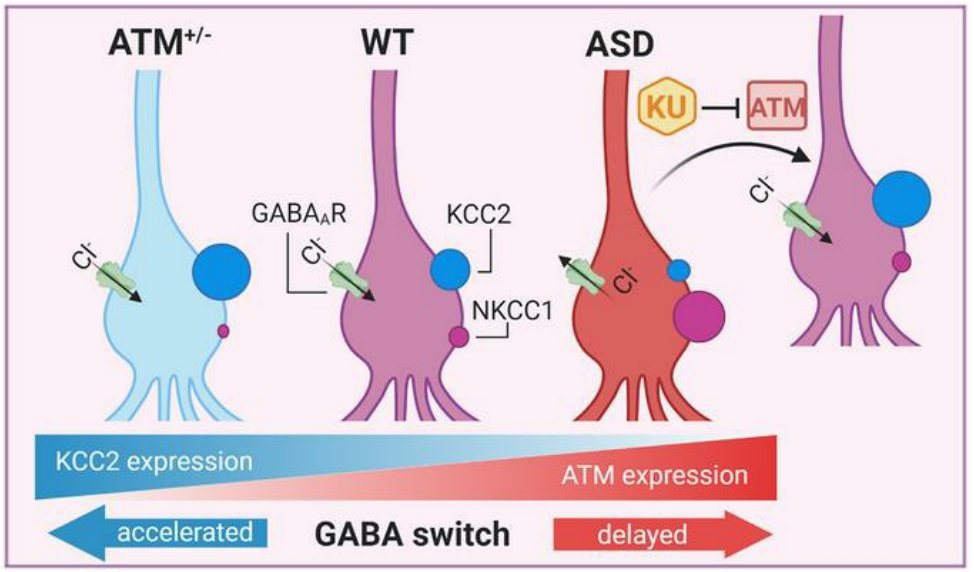

The DNA repair protein ATM as target in autism spectrum disorder

Lara Pizzamiglio[1], Elisa Focchi[1], Clara Cambria[1], Luisa Ponzoni[2], Silvia Ferrara[1], Francesco Biari[1], Genni Desiato[3], Nicoletta Landsberger[1], Luca Murru[2], Maria Passafaro[2], Mariaelvina Sala[2], Michela Matteoli[3,2], Elisabetta Menna[3,2] and Flavia Antonucci[1]*

1 Department of Medical Biotechnology and Translational Medicine (BIOMETRA), University of Milan, Milano, Italy; 2 Institute of Neuroscience, IN-CNR, Milano, Italy; 3 Humanitas Clinical and Research Center - IRCCS, Rozzano, Milan, Italy.

Corresponding author:

*Flavia Antonucci: Department of Medical Biotechnology and Translational Medicine, University of Milan, via Vanvitelli 32, 20129, Milan - Italy phone: 0039 0250317095; mail: Flavia.Antonucci@unimi.it

Short title: ATM activity in autism

Keywords: ATM blockade; inhibition; neurodevelopmental disorders; drug repositioning.

ABSTRACT

Impairment of GABAergic system has been reported in epilepsy, autism, ADHD and schizophrenia. We recently demonstrated that Ataxia Telangiectasia Mutated (ATM) shapes directly the development of GABAergic system. Here, we show for the first time how the abnormal expression of ATM impacts the pathological condition of autism. We exploit two different animal models of autism, the *Mecp2*$^{y/-}$ mouse model of Rett syndrome, and mice prenatally exposed to valproic acid, and found increased ATM levels. Accordingly, the treatment with the specific ATM kinase inhibitor KU55933 (KU) normalises molecular, functional and behavioural defects in these mouse models such as the i) delayed GABAergic development, ii) hippocampal hyper-excitability, iii) low cognitive performances, iv) social impairments. Mechanistically, we demonstrate that KU administration to wild type hippocampal neurons leads to i) higher Egr4 activity on *Kcc2b* promoter, ii) increased expression of Mecp2, iii) potentiated GABA-transmission. These results provide evidences and molecular substrates for the pharmacological development of ATM inhibition in autism spectrum disorders.

INTRODUCTION

In several developmental diseases such as autism, Down syndrome, Dravet syndrome, Rett syndrome, perinatal neuroinflammation and epilepsy, an altered GABA-mediated inhibition has been addressed [1-5], as well as an imbalanced excitatory-inhibitory ratio (E/I balance) [6-8]. In fact, whereas glutamate mediates neuronal depolarization along life, at the early stages of neuronal development, GABA acts as an excitatory neurotransmitter rather than inhibitory [9-13], directly evoking action potentials and raising intracellular calcium levels ($[Ca^{2+}]_{in}$) [12, 14, 15]. This excitatory action of GABA depends on the expression of the sodium-potassium-chloride cotransporter NKCC1, which maintains the intracellular chloride concentration high in immature neurons [9]. Then, during neuronal development, it acquires its typical role of brake for neuronal activity through the important process called "excitatory-to-inhibitory switch of GABA" (also called GABA-switch), which is directly related to the action of the potassium-chloride co-transporter KCC2. By extruding the chloride from neurons, KCC2 guarantees i) a low intracellular ion concentration and ii) the inhibitory function of GABA upon the opening of GABA-A receptor. In line with these pivotal effects, impaired KCC2 expression or function associate to the generation of neurodevelopmental diseases and, accordingly, KCC2 enhancement is at the basis of the new therapeutic strategy for these conditions [16].

Recently, we demonstrated that neurons expressing reduced levels of Ataxia Telangiectasia Mutated (ATM), a protein involved in the DNA double strand breaks (DSBs) response, display increased KCC2 levels, premature GABA-switch and higher inhibitory tone [17]. Moreover, several findings highlight ATM important involvement in fundamental neurobiological processes such as neuronal survival, cellular proliferation and synaptic vesicles recycling [18-21]. Also, a proper functioning of DSBs machinery [22] is necessary for proper development of cognitive abilities [23]. Interestingly, a recent study identified 11 candidate single-nucleotide polymorphisms (SNPs) and 6 genes contributing to Attention Deficit Hyperactive Disorder (ADHD) susceptibility and among these the *ATM* gene is included [24]. Also, in a Taiwanese Han population, a specific Runs of homozygosity (ROH) region associated with the language impairments of autism has been found on 11q22.3 chromosome, a region which contains the ATM gene [25]. Thus, these genetic studies support a role of ATM in the aetiology of developmental disorders.

Considering all above, we hypothesized that the tuning of ATM kinase activity could be beneficial in neurodevelopmental pathologies and, to this scope, we investigated the effects of the ATM kinase inhibitor, KU55933 (KU). Here, we describe the capacity of KU to recover neuronal alterations found in *Mecp2* null (*Mecp2*$^{y/-}$) neurons and in mice exposed to valproate (animals in utero exposed to VPA, VPA-mice). Both are considered good models of autism spectrum disorders (ASD) and are characterized by a prolonged excitatory GABA action and hyperexcitability. Coherently, both models present, among the aetiopathological alterations, reduced KCC2 levels [26-30]. Also, we demonstrate that the higher KCC2 expression achieved by the inhibition of ATM kinase occurs through i) the promotion of the activity of the immediately early gene

Egr4 on *Kcc2b* promoter and ii) the increased expression of the epigenetic regulator Mecp2. Accordingly, both mechanisms result potentiated in *Atm* heterozygous neurons and tissues.

Thus, we highlight a completely new and unexplored application of KU in neurodevelopmental disorders since up to now it has been studied as an antiproliferative and radiosensitizer agent against tumours [31, 32] [31, 33, 34]. It is a small molecule possibly able to generate unspecific actions, but here we also identified the lowest concentration able to guarantee both safety and effectiveness in neurons.

This study indicates that the inhibition of ATM kinase activity, achieved by KU, may revert functional features in autism by the restoration of the proper development of inhibition and by preventing the occurrence of deleterious effects linked to neuronal hyperexcitability driven by an excitatory GABA action.

RESULTS

ATM expression is higher in hippocampal tissues of two animal models of autism

In order to unveil the possible involvement of ATM in ASD we took advantage of two different animal models: the *Mecp2*$^{y/-}$ mice and mice prenatally exposed to valproic acid (VPA), as genetically- and pharmacologically-linked models of autism**.** As illustrated in Fig 1A, we found increased amount of ATM in hippocampi of *Mecp2*$^{y/-}$ pups (P6) as well as in hippocampi of young VPA animals (Fig 1B), i.e. mice generated by pregnant dams injected with VPA (600 mg/ml ip) at GD 12,5. *Vice versa*, in *Atm*$^{+/-}$, Mecp2 expression is higher with respect to age and sex matched wt mice (Fig 1C), suggesting a possible reciprocal correlation between the two proteins. Also, whereas *Atm*$^{+/-}$ hippocampi displayed a higher expression of KCC2 [17], in *Mecp2*$^{y/-}$ and VPA mouse models of autism a lower level of KCC2 has been described [26, 28, 30]. Thus, starting by these premises, here we investigated the effects of ATM kinase inhibition *in vitro* and *in vivo* both in wt mice and animal models of autism.

ATM kinase inhibitor KU boosts KCC2 expression in vitro and in vivo, anticipates the excitatory-to-inhibitory GABA switch and potentiates inhibitory neurotransmission

First of all, we asked whether in vivo pharmacological blockade of ATM may affect KCC2 levels. Accordingly with literature [32, 35, 36], we injected 3 µl of KU 10 µM in the single lateral ventricle of P3-4 WT mice (Fig 2A) and quantified KCC2 expression 1-2 days later by Western Blotting analyses. As showed in Fig 2B, a higher KCC2 expression was found in KU-treated mice. It has been reported that doses higher than KU 2 µM inhibit autophagosome formation [37], so we evaluated the impact of this treatment on basal autophagy *in vivo*. As marker of autophagy, we looked at the microtubule-associated protein 1 light chain 3, BII isoform (LC3-BII) in brains explanted from KU-injected pups. Western Blotting results indicated that levels of LC3-BII are not affected by KU treatment (Fig 2C, bottom). Also, a comparable result was obtained evaluating levels of HSPA8 (Fig 2C, above), which is an ubiquitous molecular chaperone involved in protein folding and degradation, stress response, endosomal microautophagy, and chaperone-mediated autophagy [38, 39].

In vitro, we evaluated KU effectiveness, duration of action and toxicity in control primary cultures (see Supplementary Materials and Suppl. Fig 1A-F). We identified the lower concentration able to produce the desired effects without affecting neuronal health (KU 1 µM) and we daily treated hippocampal cultures starting from 6 to 10 days in vitro (DIV) with KU 1 µM (Fig 2D). As described in $Atm^{+/-}$ hippocampal cultures [17], also neurons treated with KU displayed an increased ERK1/2 phosphorylation suggesting the occurrence of common molecular pathways (Suppl Fig 1G). *In vitro*, we detected an increased KCC2 expression 60 minutes after neuronal exposure to the drug (Fig 2E) up to 1 day (Fig 2F-left), as indicated by Western Blotting analysis. Surprisingly, KCC2 levels remained comparable to those found in DMSO/control neurons in the case of: i) long-lasting treatment, i.e upon a chronic KU administration (Fig 2F-right); ii) long and short treatments in mature cells (Suppl Fig 2H). These data suggested that the higher KCC2 expression triggered by the ATM kinase activity blockade is more likely restricted to the first phase of development whereas does not occur in mature neurons.

It is known that changes in KCC2 expression impact on GABAergic development by shaping the timing of the GABA-switch [2, 3, 9, 17, 40]. So, we expected to find a modified GABA-switch in KU neurons since the higher KCC2 expression. To address this point, we carried out calcium imaging experiments in cultures loaded with the calcium indicator FURA-2. We treated 5-6 DIV neurons with KU (Fig 2G) and evaluated the GABA-switch one day later. In particular, we measured number of neurons excited by GABA delivery and the related entity of calcium transients. Imaging experiments clearly indicated that the delivery of exogenous GABA (100 µM) generates a depolarizing response in a lower % of cells in the KU condition (Fig 2 H-I). Interestingly, this short application of KU was responsible for a long-lasting effect since the percentage of neurons depolarized by GABA was still reduced 4 days after KU treatment (Fig 2J). Since these results might reflect differences in Voltage Operated Calcium Channels (VOCC) expression we analysed calcium transients induced by the application of a different depolarizing stimulus, such as KCl 50 mM. We found that KCl was able to generate comparable calcium increases in DMSO/controls and KU-treated cultures (Suppl. Fig 1I-J). This result indicated no differences in terms of VOCC expression in KU neurons respected to the DMSO/control one and confirm the specificity of GABA switch data upon KU administration.

The short KU treatment during development impacts also the basal synaptic activity. We recorded inhibitory and excitatory miniature events (mIPSCs-mEPSCs) in 14 DIV neurons (Fig 2G) treated with KU at 5-6-DIV and found an increased inhibition. Figures 2K-L display that inhibitory transmission resulted potentiated both in frequency and amplitude whereas excitatory events were decreased only in frequency. To demonstrate that these effects directly associate with the higher KCC2 expression, we exploited the specific KCC2 blocker, VU0240551 (VU 1 µM) [41], which does not affect neuronal health (Suppl. Fig 2A and B). We co-incubated wt cultures with KU (at day 5-6) and VU 1µM (Fig 2M) and we found no differences in the % of GABA-responding neurons (Fig 2N). Interestingly, we confirmed these results also in $Atm^{+/-}$ neurons upon treatment with VU. In fact, premature GABA development (Suppl Fig 2C) as well as higher I/E ratio (evaluated by recording of

mIPSCs and mEPSCs) were fully rescued by VU delivery in *Atm*$^{+/-}$ cells (VU treatment: 2-4-6-8DIV; electrophysiological recording at 13-14DIV; Suppl. Fig 2D).

KU counteracts the pharmacologically-induced hyperexcitability in neurons

In a good accordance to the significant enhancement of inhibitory activity found in 13-14DIV neurons treated with KU at 5-6DIV, also immunofluorescence analysis revealed a higher mean intensity and mean size of vGAT-positive puncta and reduced vGlut positive signal (Suppl. Fig 3A-B). Moreover, we found that KU-treated cells were also less susceptible to a paradigm of hyperexcitability acutely generated in vitro by exposing neurons to a Mg^{++} free external medium, i.e. sustaining NMDA receptors activation [42, 43]. Multi-Unit (MU) activity, that is known to reflect the spiking activity of principal neurons [44], was recorded by voltage-clamp in the cell attached modality. This method allows to monitor the spiking activity of the recorded neuron as well as of its immediate neighbours [44]. As shown in Fig 3C, while the MU number was significantly higher in 14DIV neurons exposed to the Mg^{++} free medium respect to normal KRH, no increment in the MU frequency (Fig 3C-D) has been observed after Mg^{++} removal in neurons treated with KU at 5-6DIV. We excluded that this effect resulted from a reduction of NMDA-Receptor (NMDA-R) subunits expression (NR1, NR2A and NR2B), as indicated by Western Blotting data (Fig 3E-F).

KU mediates the rapid Egr4-dependent activation of the *Kcc2b* promoter and *Mecp2* transcription

To investigate the underlying molecular mechanisms, we explored the possibility that the enhanced *Kcc2* transcription upon KU delivery could be mediated through the activation of Egr4 as in [45]. To this purpose we used a construct including the -309/+42 region of the *Kcc2b* mouse promoter, containing exclusively the Egr4 consensus sequence, as previously demonstrated [46, 47], followed by the NanoLuc luciferase gene reporter. We transfected 5DIV control cultures with the construct, we applied KU 1 day later and we measured the Nano-Luc and Luc2 luciferase activity by a Dual-Luciferase Reporter Assay System after 24 hours. We measured an increased Luciferase Egr4 activity in KU treated cultures (Fig 4A, above) in the presence of unchanged Egr4 expression levels (Fig 4B), indicating that the higher KCC2 expression may occur through the rapid Egr4-dependent activation of the *Kcc2b* promoter. Also, 5DIV *Atm*$^{+/-}$ cultures displayed a significantly higher Egr4-dependent activity of the reporter gene with respect to age-matched wt cultures as assessed by Dual-Luciferase Reporter Assay System (Fig 4A, bottom), indicating an enhanced Egr4 activity also in the genetic model expressing reduced level of ATM protein.

Then, based on the result that Mecp2 is highly expressed in *Atm*$^{+/-}$ tissues (see Fig 1C), we evaluated Mecp2 levels in brain tissues of wt pups injected with 3 µL of KU 10 µM. Increased levels of Mecp2 signal were detected in KU-injected brains with respect to controls, as assessed either by Western Blotting analysis or confocal analysis (Fig 4C-D). Quantitative analysis for *Mecp2*-mRNA levels by qRT-PCR indicated that *Mecp2* transcription is transiently potentiated 30 and 60 minutes after KU delivery (Fig 4E). All together these results

demonstrated that KCC2 expression is finely modulated by ATM kinase activity through Egr4 and Mecp2 pathways.

KU rescues abnormal GABA switch and functional alterations in *Mecp2*$^{y/-}$ neurons

Since *Mecp2*$^{y/-}$ pups displayed higher ATM levels (see Fig 1A) and *Mecp2*$^{y/-}$ neurons showed an excitatory GABA action and low KCC2 levels [26], we tested the possibility to rescue these defects by KU treatment. A schematic representation about the experimental procedures is showed in Fig 5. Data collected by calcium imaging experiments revealed in 7-8DIV *Mecp2*$^{y/-}$ cultures that the higher percentage of GABA-responding neurons is normalized by KU delivery (Fig 5A). Once again, this effect was not linked to increased VOCC expression in the KU group since no differences in the amplitude of KCl-induced calcium responses were detectable among the groups (Fig 5B). Interestingly, in *Mecp2*$^{y/-}$neurons, the reduced calcium peaks induced by GABA delivery suggested a significant alteration in the GABA-A receptor expression, which was restored by KU application (Fig 5C). Also, the neuronal hyper-excitability induced by exposing neurons to a 0 Mg^{++} external medium has been observed only in 14DIV *Mecp2*$^{y/-}$-cultures, as indicated by the significantly higher MU frequency with respect to control solution (Fig 5D-E). No significant differences in terms of firing frequency could be detected in *Mecp2*$^{y/-}$ neurons exposed to 0 Mg^{++} solution treated with KU during development (Fig 5D-E). Accordingly, *Mecp2*$^{y/-}$ cells treated with KU displayed a potentiated Egr4 activity (Fig 5F) and normalized KCC2 levels (Fig 5G).

KU rescues abnormal GABA switch and autistic-like behaviour in VPA-mice

To address the therapeutic potentiality of KU in the valproate mouse model of autism (VPA model), we first performed *in vitro* experiments. We treated wt neurons with valproate (VPA) from 1DIV to 4DIV (see the cartoon in the Fig 6A). By calcium imaging experiments we found a higher percentage of neurons which respond to exogenous GABA with a neuronal depolarization. This defect was fully normalized by KU treatment (Fig 6B). Once again, no changes in VOCC expression occurred in KU group as suggested by the comparable amplitudes of KCl-induced calcium responses among the KU-treated and vehicle- VPA cells (Suppl. Fig 4A).

Finally, we moved to *in vivo* experiments to evaluate KU effects in the valproate mouse model of autism, since these mice display a delayed GABA switch, a long-lasting excitatory action of GABA [29] and higher ATM levels (see Fig 1B). We treated pregnant dams at gestational day (GD) 12.5 with VPA (or saline) in order to induce an autistic-like phenotype in the generated offspring ("VPA-mice"; see Fig 6C) [48, 49]. According to published data, VPA-mice display a growth delay as indicated by the reduced body weight, delayed eye opening and important defects in a battery of behaviours (Suppl. Fig 4B) such as communicative behaviour, cognitive function and social performances [48]. Communication generates by the integration of multiple information as those triggers by olfaction [50], so we evaluated the olfactory motivation test/nest bedding

test in saline- and VPA-mice. As expected, VPA animals displayed significant impairments in the % of arrivals at home cage bedding (Suppl. Fig 4B). Also, VPA mice displayed important defects in cognitive function and social behaviour that we evaluated, respectively, by the spontaneous alternation test and the sociability test (Fig 6D-E). [29]. So, we treated young adults VPA-mice with KU and assess its effects by behaviour and biochemistry. We delivered KU in VPA-mice by the intranasal route (KU 10 mM; 7,5mg/Kg; see Fig 6C) and found 2-3 days later the complete restoration of cognitive defects as well as impairments in sociability (Fig 6F-G). Since the GABA -inhibitory or -excitatory effects arise from the expression levels of both chloride cotransporters KCC2 and NKCC1 which complementary regulate intracellular chloride fluxes and GABA direction/response [9], we measured KCC2 and NKCC1 levels in the VPA model. As found for KCC2, also NKCC1 expression appears marginally altered in the VPA mice but analysis of the NKCC1/KCC2 ratio, which is more informative in terms of excitatory or inhibitory GABA action, reveals a significantly increment in VPA animals restored by the intranasal treatment with KU (Fig 6H).

Notably, we have identified a suitable treatment for autism, but further experiments should be performed to assess whether the beneficial effect on ASD core symptoms is also long lasting.

Altogether these data strongly indicate that KU treatment is able to ameliorate autistic traits in VPA mice and that the pharmacological tuning of ATM activity could be exploited in ASD treatment.

DISCUSSION

In this study we demonstrated that the targeting of ATM kinase activity can be exploited to normalize neuronal development and brain function. In particular, we provided the proof of principle that the application of ATM kinase inhibitor KU55933 (KU) generates a higher activation of the transcription factor Egr4 and a higher transcription and expression of the epigenetic regulator Mecp2 determining increased KCC2 levels (see the cartoon in Fig 7). Consequently, it promotes the development of GABAergic system and, through the trophic action of the GABA itself, an increased inhibitory transmission. Therefore it may be used to treat pathological conditions characterized by KCC2 deficiency [1-3, 51, 52]. KU is already used in pre-clinical studies for cancer treatment [31, 35, 36]. It is a small molecule with possible undesirable side effects depending on the dosage and route of administration. We identified the lowest concentration free from toxic effects for the in vitro and in vivo experiments and by the intranasal delivery we basically exclude systemic effects. Several studies indicate that KU displays a good selectivity for the ATM kinase, in fact: i) 10 mM KU has no significant effects on unspecific pathways such as the CREB transcriptional basal activity [53]; ii) the dose of 5 µM KU is the highest non-toxic drug concentrations linked to a cell viability >85% [54]; iii) 2 µM KU does not inhibit the cell survival [37]; iv) 2 µM KU inhibits rapamycin-induced autophagosome formation and amino acid starvation-induced autophagic flux in cell lines [37]. Since we used 10 µM KU in vivo experiments we checked the possible KU-inhibition of basal autophagy by measuring levels of autophagy markers such as LC3-BII protein and of endosomal microautophagy, and chaperone-mediated autophagy, HSP8A protein. We

did not find any changes in these proteins expression even if KU concentration applied in vivo is much higher respect to the one linked to the autophagy inhibition found in vitro. We justify these results by the evidence that i) in ventricle KU gets diluted, thus the effective concentration is lower respect to the injected one; ii) starting by the same drug concentration different effects can be induced in different protocol (in vivo vs in vitro); iii) the inhibition of autophagosome formation has been proved for KU in an autophagy-activated protocol whereas we evaluate KU effects in un-stimulated neurons/mice.

In a previous study we showed a novel role of ATM in the regulation of the development of GABAergic inhibition [17]. Here we investigate whether, and to what extent, the ATM kinase activity impacts neurotransmission during physiological brain development and in neurodevelopmental disorders. Our in vitro results corroborate the link between ATM activity and KCC2/NKCC1 expression and clarify that among the ATM functions there is the control of NKCC1/KCC2 balance thus resulting in a new biological substrate to target in developmental disorders affected by NKCC1/KCC2 deregulation. Importantly, here we demonstrate that ATM activity plays an essential role in the maturation of GABAergic system leveraging on 2 transcription factors, Mecp2 and Egr4, which control the expression levels of several proteins among which KCC2. In fact, with a reduced but still present ATM activity (i.e. KU treated cells/mice and in *Atm*-Het neurons/mice), these two factors nicely work leading to correct KCC2 levels. *Vice versa*, in Mecp2-null brains, in which we found higher ATM expression, KCC2 is reduced and KU administration normalizes its expression potentiating Egr4 activity. Thus, variations in ATM levels or activity reflect opposed KCC2 expression and alteration in GABAergic development based on Egr4- and Mecp2-dependent mechanisms.

Our findings acquire particular relevance since cognitive dysfunctions in psychiatric and neurodevelopmental disorders have been recently linked to proteins involved in DNA double-strand breaks (DSBs) machinery [22, 55-57]. In particular, it has been demonstrated that neuronal responses to external stimulation is associated to the formation of DSBs [55, 56]. Exposure of mice to physiological learning behaviours results in activity-induced DSBs restricted to loci enriched for the early response genes, including *Fos, Npas4, Egr1,* and *Nr4a1* [22, 23] which may impact synaptic function by epigenetic mechanisms. In this scenario, these studies, including our present results, demonstrate that defective repair DSBs factors generate neurological abnormalities and that a better understanding of mechanisms underlying these alterations will be of enormous significance.

Also, several animal models demonstrated that increased excitatory/inhibitory balance occurs in a large case of psychiatric pathologies resulting from genetic modifications, as indicated in: *i) $Oxt^{-/-}$ or $Scn1a^{+/-}$* animals (the mouse models of myoclonic-epilepsy associated to autistic behaviour [5, 58]), ii) FMRP mice (genetic animal model of Fragile-X syndrome/mental retardation [59]), iii) REELER mouse model of schizophrenia [60, 61] vi) *$Mecp^{y/-}$* mice for Rett syndrome [62, 63] and v) in the pharmacological-induced VPA model. Our findings highlight ATM kinase as a new potential target for restoring the proper equilibrium between the glutamatergic and GABAergic afferents in conditions characterized by hyperactivity. Indeed, results collected

here in *Mecp2*$^{y/-}$ neurons and VPA model indicate that the ATM tuning positively impacts on defective neuronal development leading to a normal GABAergic maturation and function. Finally, ATM signalling has been found consistently elevated in cells derived from Huntington mice and in brain tissues from Huntington mice and patients. Notably, the reduction of ATM expression, obtained by crossing the murine *Atm* heterozygous null allele onto mice expressing full-length human Huntington ameliorates multiple behavioural deficits and partially improves neuropathology in the Huntington mouse model [64, 65]. Also, in two mouse models for Huntington disease, the cognitive defects have been demonstrated to be linked to a reduced KCC2 expression that generate a condition of excitatory GABA [65]. These results further support our hypothesis of placing ATM among the pathways responsible for the correct development of the central nervous system.

Our data indicate that among the pathological modifications occurred in the mouse models of autism such as in *Mecp2*$^{y/-}$ mice and in VPA-model, a higher ATM activity contribute to the generation of the altered neuronal phenotype. Further experiments are needed to better investigate the involvement of ATM in other neurological state such as autism and epilepsy since these pathologies may result from insufficient KCC2 levels and hyperexcitability. In particular, KU application in developmental diseases offers, as a positive example of drug repositioning, the big benefit to shorten time of drug characterization and to develop an old drug in a new field.

MATERIALS AND METHODS

Animals

All efforts were made to minimize the number of animals used and their sufferings. Mice were maintained under standard laboratory conditions [room temperature (22 ± 2 °C) with 12:12 h light: dark cycle (lights on at 8.00 AM) with food and water *ad libitum*] and kept 5 per cage. Tests were conducted during the light phase of the circadian cycle between 9.00 AM and 1.00 PM. *Atm* heterozygous mice were generated crossing *Atm* heterozygous males and C57BL/6 females, *Mecp2-null* mice were provided by Prof Nicoletta Landsberger and pregnant C57BL/6 dams were purchased from Charles River.

Cell cultures

Characterization of KU55933 was conducted on hippocampal neurons established from E18 rat littermates as described previously [66]. *Atm* genetically-modified cultures were established from E18 embryos; *Mecp2* genetically-modified neuronal preparations were obtained by Postnatal day 0 (P0) pups in order to minimize number of pregnant females sacrificed [17].

Genotyping

Genotyping for *Atm* and *Mecp2* animals was performed using polymerase chain reaction (PCR) techniques. After DNA purification [67], 3 µl of DNA were added to: 7,5 µl of master mix (GoTaq Promega), 0,25 µl of each primer and 3,75 µl of Nulcease free water for *Atm* genotyping and 7,5 µl master mix (GoTaq Promega), 0,375 µl of each primer and 3,375 µl of Nuclease free water for *Mecp2*. The DNA was amplified using thermocycler (Biorad, Hercules, CA, United States). Primers Sequences for *Atm* genotyping: 5'-GTAGTAACTATTAGTTTCGTGCA-3', 5'-TAGGGTGTAGTAGTGGAGGA-3', 5'-ACGTAAACTCGTCTTCAGACCT-3'. Primers Sequences for *Mecp2* genotyping: 5'-CCACCCTCCAGTTTGGTTTA-3' as reverse primer, 5'-ACCTAGCCTGCCTGTACTTT-3' as forward primer for *Mecp2* null allele and 5'-GACTGAAGTTACAGATGGTTGTG-3' as forward primer for wt allele [68].

Western Blotting

Proteins were extracted starting from explanted tissues or scraped neurons using lysis buffer containing sodium dodecyl sulphate 1% (SDS), 62.5 mM Tris-HCl (pH 6.8), 290 mM sucrose for tissues and sample buffer containing 3% SDS, 115 mM sucrose, 65mM Tris-HCl (pH 6.8), 0,1 % βmercaptoethanol for cells. The total protein concentration of the samples was assessed with a protein assay kit (Thermo Fisher Scientific) using a bovine serum albumin-based standard curve. Protein extracts from tissues or neurons were separated by SDS-PAGE electrophoresis and blotted. Homogenates from cortices and/or hippocampi obtained from P4 wt pups (injected or not with KU), P7 $Mecp2^{y/-}$ vs wt male mice, $Atm^{+/-}$ vs wt and VPA-mice vs sal-mice were analysed by western blotting using: rabbit anti-KCC2 1:1000 (Millipore 07-432), rabbit anti-ATM 1:500 (Millipore 071286), rabbit anti-Mecp2 1:1000 (Sigma-Aldrich M9317), rabbit anti-LC3B1/2 1:1000 (Cell Signaling D11) and HSPA8 1:1000 (Cell Signaling D12F2) antibodies. For scraped neurons mouse anti-p-ERK 1:1000 (Sigma-Aldrich E7028), rabbit anti-ERK1/2 1:1000 (Cell Signaling 9102), rabbit anti-KCC2 1:1000 (Millipore 07-432), rabbit anti-Egr4 1:1000 (Abcam ab198197); mouse anti-NMDA-R1 1:500 (Synaptic System 114-011); rabbit anti-NMDA-R-2A: 1:500 (Millipore 05-901R); mouse anti-NMDA-2B 1:1000 (NeuroMab 75-101). HRP-conjugated secondary antibody 1:40000 (Jackson ImmunoResearch) were used. Immunoreactive bands were detected by using the Pierce ECL Western Blotting Substrate (Thermo Fisher Scientific Inc., Rockford, IL), and analysed with Image J software. Rabbit anti-calnexin 1:1000 (Sigma-Aldrich C4731), mouse anti-actin 1:1000 (Sigma-Aldrich A4700) or mouse anti-βIII-tubulin 1:2000 (Promega G712A) was used as loading controls.

Calcium imaging

Hippocampal neurons were loaded with the membrane-permeable fluorescent Ca^{2+} indicator Fura2-AM (1 µM; Sigma-Aldrich) for 30 min at 37°C, 5% CO2; cells were then washed with KRH buffer (NaCl 125 mM, KCl 5 mM, MgSO4 1.2 mM, KH2PO4 1.2 mM, CaCl2 2 mM, Hepes 25 mM; D-Glucose 6 mM) and placed into the recording chamber of an inverted microscope (Axiovert 100, Zeiss) equipped with a calcium imaging unit and

imaged through a 40x objective (Zeiss). Fura-2AM was excited at 380 nm and at 340 nm through a Polychrom V, (TILL Photonics GmbH) controlled by the TillVisION software 4.01. Emitted light was acquired at 505 nm at 1Hz, and images collected with a CCD Imago-QE camera (TILL Photonics GmbH). Calcium transients have been addressed by evaluating the fluorescence ratio F340/380. This parameter was recorded in regions of interest (ROIs) corresponding to neuronal cell bodies and analysed along sequential images to follow temporal changes.

Basically, after a period of basal recording, GABA was administered at 100 µM concentration and increments in F340/380 ratio (ΔF340/380, which represents calcium transient), were considered if higher than 0.05 units. Transients occurring within 5 s after drug administration were considered actual calcium responses. After GABA administration neurons were washed with KRH and let recover few minutes, then KCl 50 mM was administered to identify viable neurons. Neurons responding to depolarization delivery with a ΔF340/380 smaller than 0.1 units were excluded from the analysis.

In vitro electrophysiology

The ATM kinase inhibitor KU55933 10 mM dissolved in DMSO (used at final concentration of 1µM) has been applied for 4 consecutive days (staring from 7-to-11DIV neurons) without changing the neuronal medium and electrophysiological properties were evaluated on 12DIV cells. In the acute treatment protocol, we treated neurons with KU at 5-6DIV and we evaluate activity in 13-14DIV neurons. Excitatory and inhibitory post-synaptic currents in miniature (mEPSCs and mIPSCs) were measured by whole cell patch clamp procedure using an Axopatch 200A amplifier (Axon Instruments, Forest City, CA, USA) in the voltage-clamp mode. mEPSCs and mIPSCs were sampled at 10 kHz and filtered at 2-5 kHz. External solution [Krebs-Ringer's-HEPES] consisted of (in mM): 125 NaCl, 5 KCl, 1.2 $MgSO_4$, 1.2 KH_2PO_4, 2 $CaCl_2$, 6 glucose, and 25 HEPES-NaOH (pH 7.4). Postsynaptic events were recorded in the presence of 1 µM tetrodotoxin (TTX; Tocris Bioscience, Bristol, United Kingdom). Recording pipettes were pulled from capillary glass (World Precision Instruments, Sarasota, FL, USA) using a two-stage puller (Narishige, London, United Kingdom), and had tip resistances of 3-5 Mohm when filled with intracellular solution (in mM): 130 Cs-gluconate, 8 CsCl, 2 NaCl, 10 HEPES, 4 EGTA, 4 MgATP and 0.3 Tris-GTP. Voltage-clamp recordings were performed at holding potentials of -70 mV and +10 mV for mEPSCs and mIPSCs, respectively. Recordings were performed at room temperature. Data were analysed off-line (pClamp-10 software, Axon Instruments). To be taken into account, mEPSCs had to exceed a threshold of 8 pA whereas for mIPSCs it has been set at 6 pA. The I/E ratio has been calculated by dividing mIPSCs and mEPSCs frequencies measured in the same neuron. MultiUnit activity (MU) has been detected in cell-attached configuration clamping neurons at -50 mV rather than -70 mV and hyperexcitability was measured applying KRH external solution with 0 Mg^{++} during the entire recording session. In this case intracellular solution is (mM): 130 K-gluconate, 10 KCl, 1 EGTA, 10 HEPES, 2 $MgCl_2$, 4 MgATP and 0.3 Tris-GTP.

Regarding data collected using the KCC2 blocker VU0240551, we used the final concentration of 1 □M (starting solution 10 mM in DMSO).

Luciferase assay

5DIV hippocampal neurons were co-transfected with pNL1.1 [Nluc] vector (Promega) containing the -309/+42 region of the *Kcc2* mouse gene and pGL4.54 [luc2/TK] vector (Promega) using Lipofectamine 2000 (Invitrogen) according to the manufacturer's protocol. 48 hours after transfection, cultures were briefly washed with PBS and lysed in Passive Lysis Buffer (Promega). Both *Nluc* and *luc2* luciferase activities were measured using Nano-Glo Dual-Luciferase Assay System (Promega).

pNL1.1 [*Nluc*] vector was modified by introducing in its multiple cloning region the -309/+42 region of *Kcc2* mouse gene containing the Egr4 consensus sequence as the only binding site for transcription factors (as described previously by [46, 47]. Cloning procedures were performed by Bio-Fab Research srl (Rome).

Immunofluorescence

P4 wt C57BL6/J pups were injected with KU 10 µM or vehicle. 24 hours after the injection pups were euthanized and the brains were removed and fixed in 4% paraformaldehyde for 48 hours. Brains were then included in 4% Low Melting Point agarose (Sigma-Aldrich) in 1X PBS. After agarose polymerization sections of 50 µm thickness were obtained using a VT1000S vibratome (Leica Microsystems). Immunofluorescent staining was carried out on free-floating sections at the level of dorsal hippocampus. Staining was performed using a primary antibody against Mecp2 (Sigma-Aldrich) followed by incubation with the specific secondary antibodies, counterstained with DAPI and mounted in Fluorsave (Merck). Images were acquired and analysed as described in [70].

Quantitative real time PCR

6DIV wt neurons were treated with KU and homogenized prior to RNA extraction using TRIzol reagent (Invitrogen). Total RNA was isolated using the Direct-zol RNA MiniPrep isolation kit (Zymo Research) according to the manufacturer's protocol. The RNA was eluted with 25 µL DNase/RNAse-free water, quantified using NANOdrop 2000c spectrophotometer (Thermo Fisher Scientific) and optical density 260/280 nm ratios were determined. Reverse transcription was performed using 1 µg RNA with a High Capacity cDNA RT kit (Applied Biosystems). Real-time polymerase chain reaction (qRT-PCR) was performed using a CFX96 thermal cycler (Bio-rad) in a final volume of 10 µl using Sybr Green technique (SensiFAST SYBR Lo-ROX, Bioline). Mecp2 was analysed at least in duplicate and data analysis was performed with the ΔΔCt method and expressed as fold change. Mecp2 mRNA levels were normalized to GAPDH.

***In vivo* KU injection**

4 days after the delivery, wt C57BL6/J pups (n=24) were anesthetized by cold-ice procedure. After 5 minutes animals received in the ventricle of the right hemisphere, a single unilateral injection of 3 μL of KU 10 μM in DMSO (n=12) or DMSO only (n=12). The day after, cortical and hippocampal tissues were explanted from both the ipsi- and contra-lateral hemispheres and stored at -20° C. Regarding the intranasal delivery, KU55933 or vehicle (DMSO) has been administered to P40 VPA/control mice by intranasal route at a dosage of 7.5 mg/kg. The mice have been previously anesthetized, and the total volume was administered 3 μl at a time, alternating the two nostrils.

Valproic acid treatment

In vitro experiments: hippocampal neurons have been treated with valproic acid (VPA, Sigma-Aldrich) 2 mM starting from 1DIV for 4 days. Then, 6DIV neurons received KU 1μM and calcium imaging experiments have been performed one day later.

In vivo experiments: pregnant wild type dams (n=5, 4-month-old) received an intraperitoneal injection of valproic acid 600 mg/kg (VPA, Sigma-Aldrich) at gestation day (GD)12.5, as previously described [71, 72]. Control dams (n=4; 4-months-old) were treated with saline only. Also, 2 pregnant dams have been treated with VPA, but pups were not able to survive.

Behavioural Tests

Pups appearance: Mice were weighed at P3, P7, P10, P14, P21 and P50, weighing a random sample of 2–3 perinatal pups rather than the entire litter to prevent perinatal pup loss.

Eye opening was checked at P13-14. Pups were checked for their general appearance at each weighing time point. Number of animals are specifically indicated in the legend.

Olfactory motivation (nest bedding test): Saline- and VPA-mice were tested for olfactory motivation at P10 by placing them in the centre of a square (7 cm × 7 cm) plastic tray as previously described [73]. One corner of the tray contained bedding from the home cage while the opposite one contained new clean bedding. The home cage bedding had not been changed since the dam was at E18. Mice were placed with their heads pointed toward an empty corner of the tray, forcing it to turn left or right to orientate toward the bedding corners. Mice were allowed up to 1 minute to reach a corner, before the trial was stopped. Trials in which mice failed to move, or to arrive at a bedding corner, were considered uncompleted trials, whereas those in which mice arrived at a bedding corner within 1 min were considered completed trials. The latency to reach a bedding corner and the type of bedding corner reached were recorded for each of the three trials. After each trial the tray was rotated so the beddings were in different orientations relative to the mouse. The nest bedding arrival was calculated as the percentage of trials in which the mice reached the home cage bedding on the total of 3 trials. Number of animals are specifically indicated in the legend.

Spontaneous alternation: Saline- and VPA-mice have been tested before and after intranasal KU delivery (2-3 days later). Spontaneous alternation was measured using a Y-shaped maze constructed with three symmetrical grey solid plastic arms at a 120-degree angle (26 cm length, 10 cm width, and 15 cm height) as previously described [74]. Mice were individually placed in the centre of the maze and were allowed to freely explore the three arms for 8 minutes. Arm entry was defined as all four limbs within the arm. A triad was defined as a set of three arm entries, when each entry was in a different arm of the maze. The maze was cleaned with water and 70% ethanol between sessions to eliminate odour traces. The number of arm entries and the number of triads were recorded in order to calculate the alternation percentage (generated by dividing the number of triads by the number of possible alternations and then multiplying by 100). Number of animals are specifically indicated in the legend.

Sociability: Saline- and VPA-mice have been tested before and after intranasal KU delivery (3 days later). The apparatus was a rectangular three-chamber, transparent polycarbonate box as previously described [75]. The test mouse was first placed in the middle compartment, and it was allowed to explore all three chambers for 10 min (habituation). Then, an unfamiliar adult female mouse (never been in physical contact with the subject mouse) was placed in an empty wire cage in one side compartment whereas the opposite side contained an empty wire cage. The time spent exploring the unfamiliar mouse and the empty cage was video recorded for 10 min. The sociability index (SI) was evaluated as follows: SI = (time exploring the unfamiliar mouse – time exploring the wire empty cage) / (time exploring the unfamiliar mouse + time exploring the wire empty cage). The present task was videotaped and then the parameter scored by an experimenter blind to the treatment offline. Number of animals are specifically indicated in the legend.

Statistics

Data were processed by SigmaStat (Systat Software Inc., San José, CA). The normal distribution of experimental data was assessed using D'Agostino-Pearson normality test. For normally distributed data Student's t-test and ordinary one-way Anova with Holm-Sidak's multiple comparisons test were performed. Mann-Whitney's rank sum test or non-parametric one-way Anova (Kruskal Wallis test and Dunn's multiple comparisons test) were applied for non-normally distributed data. Values were expressed as means ± SEM. A P value of < 0.05 was considered statistically significant.

Study approval

All the experimental procedures followed the guidelines established by the Italian Council on Animal Care and were approved by the Italian Ministry of Health (authorization n° 991/2016-PR, 369/2019-PR, 210/2017-PR).

ACKNOWLEDGMENTS

The financial support of Fondazione Telethon – Italy (Grant no. GGP16015) is gratefully acknowledged. FA is economically supported by “Piano di Sostegno alla Ricerca, PSR 2018 - Progetto giovani ricercatori”, BIOMETRA Department - University of Milan and by Italian Ministry of University and Research, PRIN 2017 (5C22WM to FA).

EM is supported by Fondazione Vodafone 2017-2018 and Progetto Bandiera Interomics 2015-2017.

MM is supported by Cariplo (2012-0560 and 2015-0594), Regione Lombardia-CNR 2017-2019, Italian Ministry of Health GR-2011-02347377 and Fondazione Vodafone 2017-2018.

NL is indebted to the Italian association of parents PRORETT research for supporting this study.

We kindly thank Dr. Roberta Benfante (IN-CNR Institute of Milan) and Dr. Simona Di Lascio (University of Milan - BIOMETRA) for helping us with the Luciferase measurements. We also thank Dr. Massimo Mantegazza for giving the opportunity to LP to conclude part of the experiments necessary for the revision.

AUTHOR CONTRIBUTIONS

LP performed calcium imaging, western blotting experiments as well as in vitro electrophysiology and analysed data, EF performed Luciferase measurements, in vivo experiments and analysed data, CC helped in blotting analysis and immunocytochemistry, LM help with electrophysiological analysis, LP performed the sociability test, SF and FB helped with KU iv injection, GD performed MQAE experiments, NL provides *Mecp2*$^{y/-}$ tissues and read the paper, MP and MS read the paper, MM and EM discussed data and read the paper, FA designed experiments, discussed data and wrote the paper.

CONFLICT OF INTEREST

The authors declare no competing financial interest.

FIGURE LEGENDS

Figure 1. Increased ATM levels in animal models of autism. A-B: ATM levels evaluated in WT (n=10) vs *Mecp2*$^{y/-}$ pups (n=13), Mann-Whitney: p=0,02; ATM levels have been measured also in offspring generated by pregnant females injected with saline or VPA at GD12.5 ("sal mice" and "VPA mice"). Sal-mice (n=12) **vs** VPA-mice (n=10), Unpaired t-test, p= 0,02. **C:** Representative Mecp2 signal and relative quantification from Western Blotting experiments performed in *Atm*$^{+/-}$ mice (wt vs *Atm*$^{+/-}$, t-test: p=0,04; number of samples: wt=5 vs *Atm*$^{+/-}$=8).

FIGURE 1

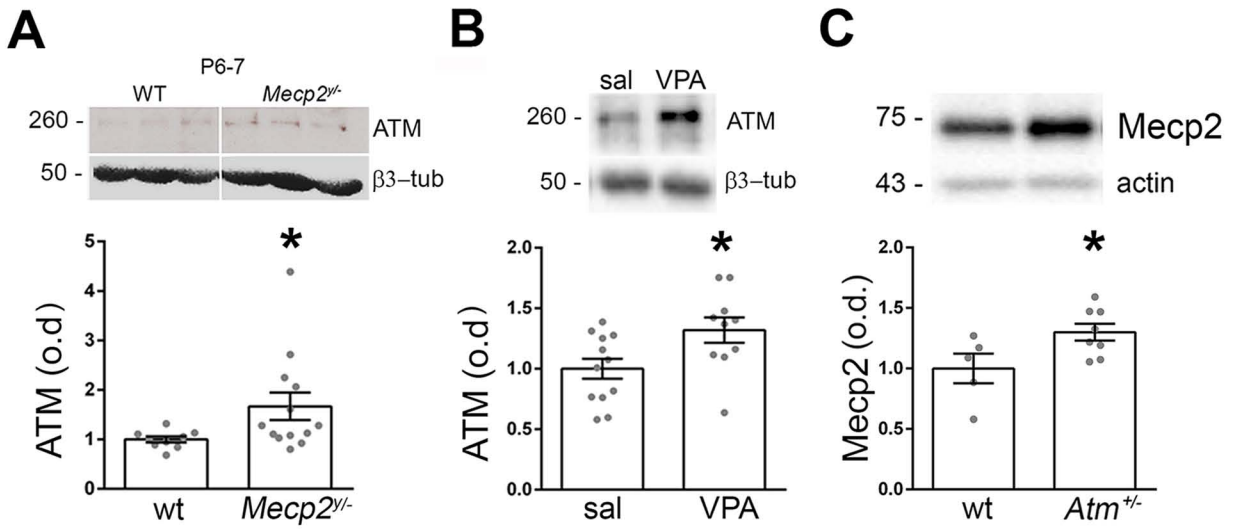

Figure 2. KU regulates GABA development and boosts KCC2 levels in vitro and in vivo. A: Representative cartoon shows the in vivo protocol to test KU-mediated effects in wt pups. **B:** Postnatal day 4 (P4) wt pups received in the right lateral ventricle a single dose of KU 10 μM (3μL) and levels of KCC2 have been evaluated in hippocampal and cortical structures one day later by Western Blotting experiments. Number of animals (DMSO=12 vs KU=12); number of cortices and hippocampi explanted and analysed: DMSO (12 ctx + 12 hippo) vs KU (11 ctx + 12 hippo); statistical analysis: Mann-Whitney: p=0.0008. **C:** In vivo KU delivery is not linked to unspecific effects as indicated by the unchanged levels of the autophagosome marker LC3-BII as well as of the endosomal microautophagy and chaperone-mediated autophagy HSP8A protein (for LC3-BII, t-test: p=0,23, number of tissues: DMSO (n=12) vs (KU=14); for HSPA8, Mann-Whitney: p=0,642; number of tissues: DMSO (n=13) vs (KU=14). **D:** The schematic representation displays the protocol of KU chronic treatment applied in wt cultures. 6DIV neurons have been treated with KU and, in a first subset of cultures, blotting experiments have been performed 30 and 60 minutes after KU delivery as well as 1 day later. In parallel, a second subset of neurons received KU for 3-4 more days and KCC2 levels have been detected at 10DIV. **E:** Increased KCC2 expression 30 and 60 min after acute KU treatment in 7DIV hippocampal neurons (for KCC2 analysis: n=7 samples per group; One-Way Anova followed by Tukey's Multiple Comparison Test: $p<0.01$). **F:** Significant increments of KCC2 levels occur up to one day after KU delivery. Number of coverslips one day after KU: CTRL=7 vs KU=11; Mann-Whitney test, p=0.005; four days after KU: CTRL=7 vs KU=11; Mann-Whitney test, p=0.918). **G:** The cartoon indicates that 5DIV neurons have been treated with KU and then tested for calcium imaging analysis at 6DIV and at 9DIV. 13DIV cells have been also recorded to measure miniature activity and fixed for immunofluorescence data. **H:** Representative traces display calcium transients in 6DIV neurons mediated by exogenous GABA application. Only neurons which display the KCl-induced response have been considered in the analysis. **I:** Evaluation of the excitatory to inhibitory switch of GABA ("GABA switch") in KU-treated cells loaded with the ratiometric calcium indicator Fura-2AM. 1 day post KU (6DIV cultures): % of GABA responding neurons: CTRL vs KU, t-test: p=0.004. Number of coverslips analysed CTRL=15 vs KU=18. Total cells analysed: CTRL=395 vs KU=374. Number of independent experiments=4. **J:** 4 days post KU (9DIV neurons): t-test: p=0.039. Number of coverslips CTRL=7 vs KU=9. Total cells analysed: CTRL=216 vs KU=236. Number of independent experiments=3. **K:** Representative electrophysiological recordings of excitatory and inhibitory post-synaptic currents in miniature (mEPSCs and mIPSCs) measured in 13-14 DIV neurons treated with KU at 5-6 DIV. **L:** Measurement of mIPSCs/mEPSCs frequency and amplitude in mature neurons treated with KU or DMSO at 5-6DIV (mIPSCs frequency: t-test p=0,0003, CTRL (n=17) vs KU (n=19); mIPSCs amplitude: t-test p=0,0469, CTRL (n=16) vs KU (n=17); mEPSCs frequency: t.test p=0,0262, CTRL (n=21) vs KU (n=17); mEPSCs amplitude: Mann-Whitney p=0,1627, CTRL (n=18) vs KU (n=16); number of independent experiments N=3, number of independent neuronal preparations N=3). **M:** The cartoon displays the experimental setting by which the direct link between "ATM

blockade, KCC2 expression and GABA development" has been demonstrated. Briefly, 6DIV neurons received both KU and VU and, since KU exerts long lasting effects, neurons received VU for additional 2 days. Then, GABA switch experiments have been carried out in 9DIV cells by calcium imaging analysis. **N:** VU administration prevents KU effects in the excitatory-to-inhibitory switch of GABA performed in 9DIV neurons. Kruskal-Wallis Test followed by Dunn's Multiple Comparisons Test: CTRL vs KU: p<0,05; KU vs KU+VU: p<0,05; ctrl vs KU+VU (n.s.). Number of fields analysed CTRL=25, KU=21, KU+VU=44. Total cells analysed: CTRL=204, KU=163, KU+VU=334. Number of independent experiments=4.

FIGURE 2

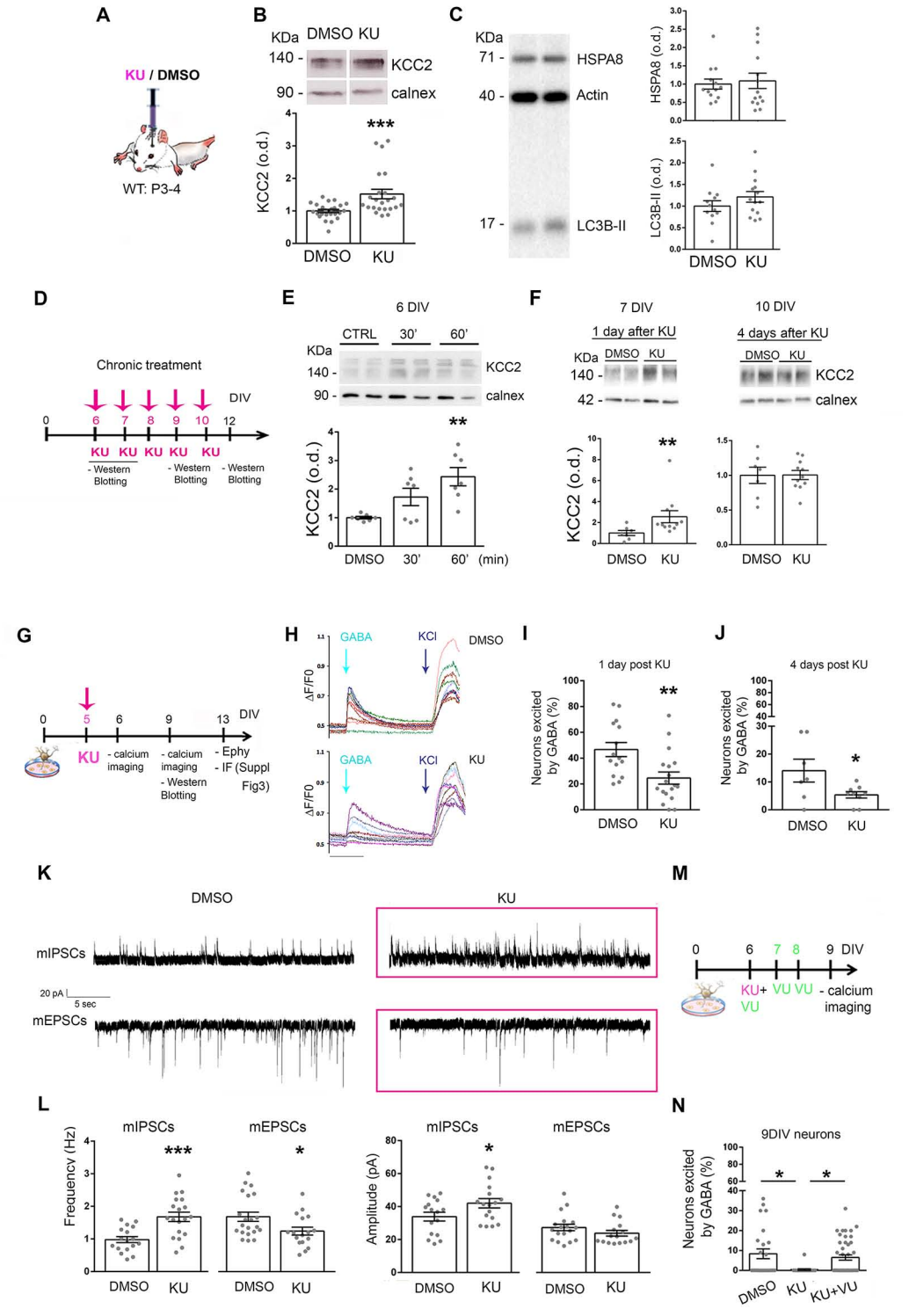

Figure 3. KU-treated cells are more inhibited and less susceptible to hyperactivity. A: Schematic representation of the experimental setting. 13-14DIV neurons, which received KU at 5-6DIV, have been tested for the hyperactivity protocol and blotting experiments. **B:** Traces of Multi-Unit (MU) activity (i.e. spiking activity) evaluated by electrophysiological recordings in the cell attached modality. Note the increased neuronal firing in mature control neurons upon Mg^{++} removal from the external solution. Neurons treated with KU at 5-6DIV result resistant to this protocol of hyper-excitability. **C:** Analysis on the MU mean frequency (Hz): One Way Anova followed by Holm-Sidak's Multiple Comparison Test: CTRL vs CTRL in Mg^{++} free sol, $p<0,001$; CTRL in Mg^{++} free sol vs KU in Mg^{++} free sol: $p<0,01$; Number of independent experiments=4. CTRL (n=34); CTRL in Mg^{++} free sol (n=28); KU (n=21); KU in Mg^{++} free sol (n=26). **D:** Each dot represents the mean of MU activity analysed per glass before and after Mg^{++} removal in the two-experimental groups (KS test<0.001). **E-F:** Blotting analysis displays no difference in NMDA-Rs expression in neurons treated with KU during development (KU treatment: 6-7DIV; Western Blotting: 14DIV neurons). NMDA-R-1: CTRL (n= 6) vs KU (n=6); t-test: p= 0,57. NMDA-R-2A: CTRL (n=5) vs KU (n=6); t-test: p=0,99. NMDA-R-2B: CTRL (n= 5) vs KU (=6); t-test: p=0,64.

FIGURE 3

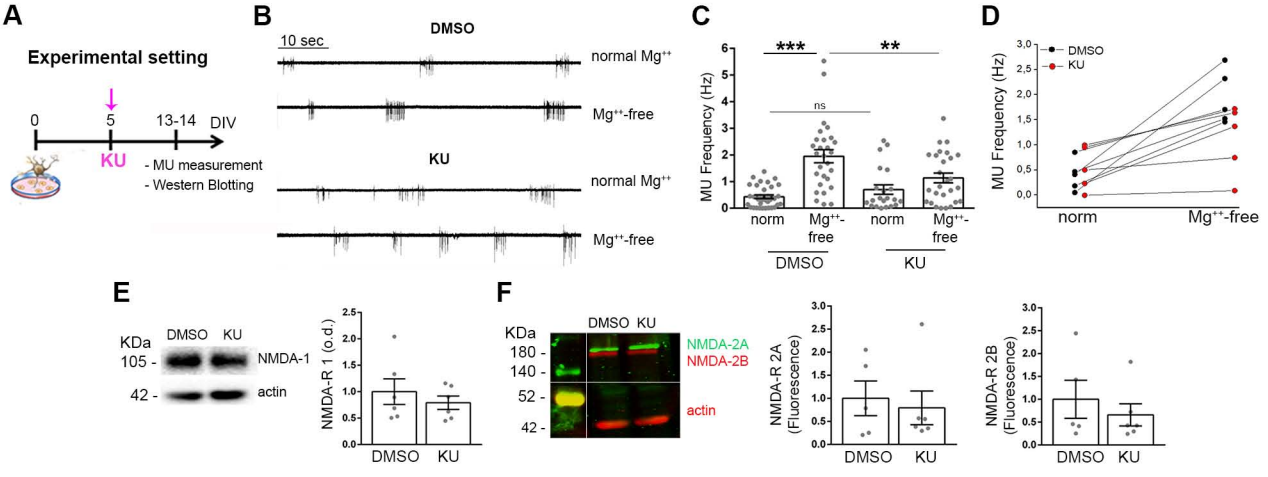

Figure 4. KU triggers Egr4 activation and increases Mecp2 transcription. A: Measurement of luciferase expression in rat cultures post KU treatment (above) and in *Atm*$^{+/-}$ cells (below). Increased Egr4 activity on *Kcc2b* promoter has been found in KU cells (NanoLuc/Luc2 normalized values, Unpaired t-test: p=0.02; number of independent experiments=3; number of samples: CTRL (n=5) vs KU (n=8)). *Atm*$^{+/-}$ cultures display also increased Egr4 activity on *Kcc2b* promoter (NanoLuc/Luc2 normalized values, Unpaired t-test: wt vs *Atm*$^{+/-}$: p<0,02; number of independent experiments=3; number of samples: wt=6, het=7). **B:** No changes occur in terms of Egr4 expression levels upon KU treatment (t-test: p=0,71; number of coverslips: DMSO=5 vs KU=6). **C:** Western Blotting experiments performed on tissues explanted from DMSO and KU-injected pups: representative Mecp2 signal and relative quantification (DMSO vs KU injected brains, t-test: p=0.01; number of tissues: DMSO=14 vs KU=15). **D:** Immuno-histological experiments for Mecp2 detection (red) at 1-day post KU injection and relative quantification in DAPI positive neurons (blue). Integrated density of fluorescence for Mecp2 signal: Mann-Whitney, p<0.0001. Number of animals: DMSO=4 vs KU=4; number of slices: DMSO=12 vs KU=12; number of images quantified per slices: 6. **E:** Quantification of *Mecp2* mRNA levels by real time PCR experiments in neurons treated with KU or DMSO at different time points (Kruskal-Wallis followed by Dunn's Multiple Comparisons Test: control neurons vs KU 30 min, p<0.001; control neurons vs KU 60 min, p<0.05).

FIGURE 4

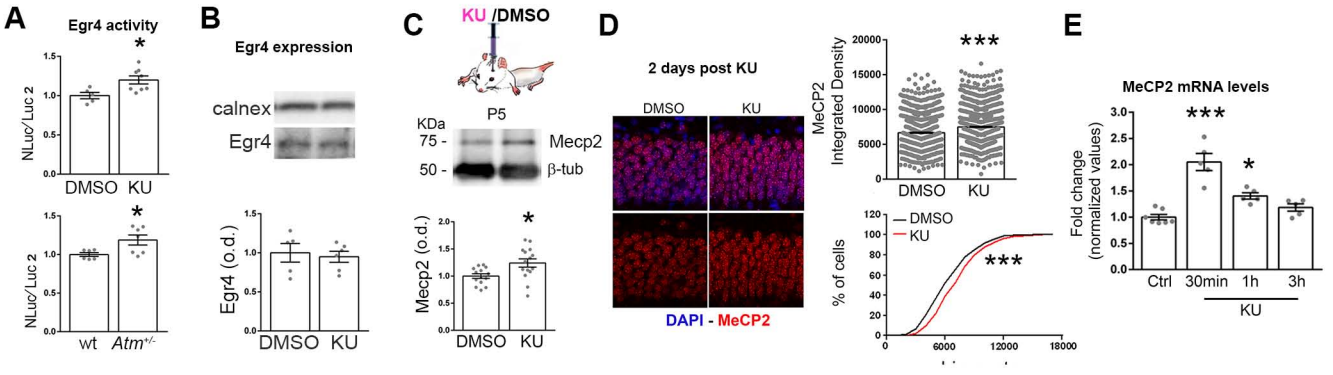

Figure 5. KU effects on *Mecp2*$^{y/-}$ developmental and functional alterations. The schematic representation indicates that 7DIV *Mecp2*$^{y/y}$ and *Mecp2*$^{y/-}$ neurons have been treated with KU (or DMSO) and calcium imaging experiments performed one day later whereas electrophysiology at 14DIV. **A:** GABA switch experiments performed in 8DIV *Mecp2*$^{y/-}$neurons and wt indicate a rescue in the % of GABA responding cells upon KU delivery (Kruskal-Wallis followed by Dunn's Multiple Comparisons Test: wt vs *Mecp2*$^{y/-}$ p<0,01; *Mecp2*$^{y/-}$ vs *Mecp2*$^{y/-}$+KU: p<0,001. Number of fields analysed wt=30, *Mecp2*$^{y/-}$=11, *Mecp2*$^{y/-}$+KU=28. Number of independent experiments=4. Total number of analysed cells: wt=227, *Mecp2*$^{y/-}$=93, *Mecp2*$^{y/-}$+KU=215). **B:** *Mecp2*$^{y/-}$ neurons treated with KU display a normal response to depolarizing stimuli induced by KCl suggesting normal VOCC expression (Kruskal-Wallis followed by Dunn's Multiple Comparisons Test: p=0.29). **C**: Calcium transients induced by GABA stimulation indicates lower amount of GABA receptors expression in *Mecp2*$^{y/-}$ cells which is also rescued by KU treatment during development (Kruskal-Wallis followed by Dunn's Multiple Comparisons Test wt vs *Mecp2*$^{y/-}$ p<0.01). **D-E:** Cell-attached experiments and quantifications display that *Mecp2*$^{y/-}$+ KU neurons are resistant in generating the pharmacological hyperexcitability induced by Mg^{++} removal (One-Way Anova followed by Sidak's Multiple Comparisons Test: *Mecp2*$^{y/-}$ vs *Mecp2*$^{y/-}$ in $0Mg^{++}$: p<0,001; number of independent experiments=3; number of cells: *Mecp2*$^{y/-}$(n=13), $0Mg^{++}$- *Mecp2*$^{y/-}$, *Mecp2*$^{y/-}$-KU (n=7), $0Mg^{++}$- *Mecp2*$^{y/-}$-KU(n=8)). **F**: KU administration potentiates Egr4 activity on the *Kcc2b* promoter in *Mecp2*$^{y/-}$ neurons as indicated by the higher NanoLuc/Luc2 value respect to the *Mecp2*$^{y/-}$ treated with only DMSO (NanoLuc/Luc2 normalized values, Ordinary One-way Anova Tukey's multiple comparison test p<0,01; number of samples (isolated embryos): wt=6, *Mecp2*$^{y/-}$+ DMSO=4, *Mecp2*$^{y/-}$+ KU=4). **G:** KU delivery increases KCC2 expression in *Mecp2*$^{y/-}$ neurons as indicated by western blotting results (One-way Anova, p=0.04; number of samples: wt=8; *Mecp2*$^{y/-}$=8; *Mecp2*$^{y/-}$+ KU=9; number of independent experiments=3).

FIGURE 5

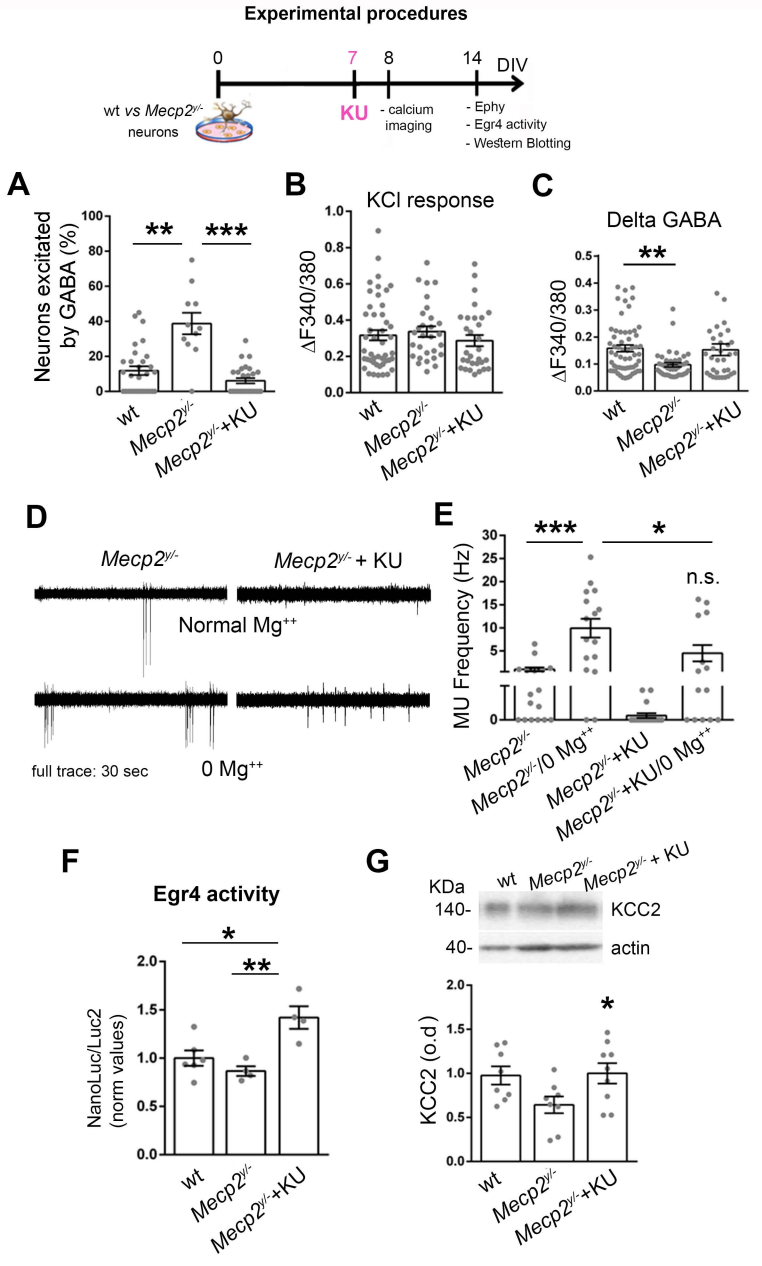
Experimental procedures
0
7
8
14
DIV
wt vs Mecp2y/- neurons
KU
- calcium imaging
- Ephy
- Egr4 activity
- Western Blotting
A
Neurons excited by GABA (%)
**
***
wt
Mecp2y/-
Mecp2y/-+KU
B
KCl response
ΔF340/380
wt
Mecp2y/-
Mecp2y/-+KU
C
Delta GABA
**
ΔF340/380
wt
Mecp2y/-
Mecp2y/-+KU
D
Mecp2y/-
Mecp2y/- + KU
Normal Mg++
full trace: 30 sec
0 Mg++
E
***
*
n.s.
MU Frequency (Hz)
Mecp2y/-
Mecp2y/-/0 Mg++
Mecp2y/-+KU
Mecp2y/-+KU/0 Mg++
F
Egr4 activity
*
**
NanoLuc/Luc2 (norm values)
wt
Mecp2y/-
Mecp2y/-+KU
G
KDa
wt
Mecp2y/-
Mecp2y/- + KU
140-
KCC2
40-
actin
KCC2 (o.d)
*
wt
Mecp2y/-
Mecp2y/-+KU

Fig 6. In vitro and in vivo effects of KU in the VPA-model of autism. A: The schematic representation displays the in vitro approach to evaluate KU effect in VPA-treated neurons. Wt cells received VPA 2mM starting from 1DIV to 4DIV as in [30]. Then 6DIV neurons have been treated with KU 1 μM and calcium imaging experiments carried out one day later. **B:** GABA switch experiments display that KU administration promotes the rescue of delayed GABA switch in VPA cultures. % of GABA responding neurons in 6DIV neurons exposed to VPA during development: Kruskal-Wallis followed by Dunn's Multiple Comparisons Test, ctrl vs VPA: $p<0,01$; VPA vs VPA+KU: $p<0,01$; number of fields analysed ctrl=24, VPA=20, VPA+KU=22; total number of analysed cells: ctrl= 237, VPA= 136, VPA+KU= 127. Number of independent experiments=3. **C:** Scheme of the experimental procedure: pregnant female (GD12.5) received VPA or saline. The generated offspring has been monitored in terms of grow delay (at P3, P7, P10, P14, P21), eye opening (P13-14), olfactory motivation/nest bedding test (P10), spontaneous alternation and sociability (P50). Then, adults receive KU or DMSO intranasally and 2-3 days later animals have been newly challenged in the spontaneous alternation test, sociability test and eventually scarified for biochemistry. **D:** Spontaneous Alteration test (analysis performed on M): % of alternation, t-test, p=0,01; number of animals: sal=11 vs VPS=11. **E:** Sociability test: social index (analysis performed on F) t-test, p=0,03; number of animals: sal=5 vs VPS=6. **F**: Spontaneous Alteration test post KU: % of alternation sal vs sal+DMSO paired t-test: p=0,92; VPA vs VPA+KU paired t-test: p=0,04; number of animals: sal (which then received DMSO, i.e sal+DMSO)=10 vs VPA (which then received KU; i.e VPA+KU)=8. **G:** Sociability Index post KU: sal vs sal+DMSO paired t-test: p=0,47; VPA vs VPA+KU unpaired t-test: p=0,04; number of animals: sal (which then received DMSO, i.e sal+DMSO)=5 vs VPA (which then received KU; i.e VPA+KU)=4. **H:** Western Blotting experiments performed on tissues explanted from adults control mice (sal+DMSO), VPA+DMSO and VPA+KU-treated adult animals: representative NKCC1 and KCC2 signals and relative quantification (One-Way Anova followed by Tukey's Multiple Comparisons Test p=0,011; number of animals: sal+DMSO=7, VPA+DMSO=10, VPA+KU=8).

FIGURE 6

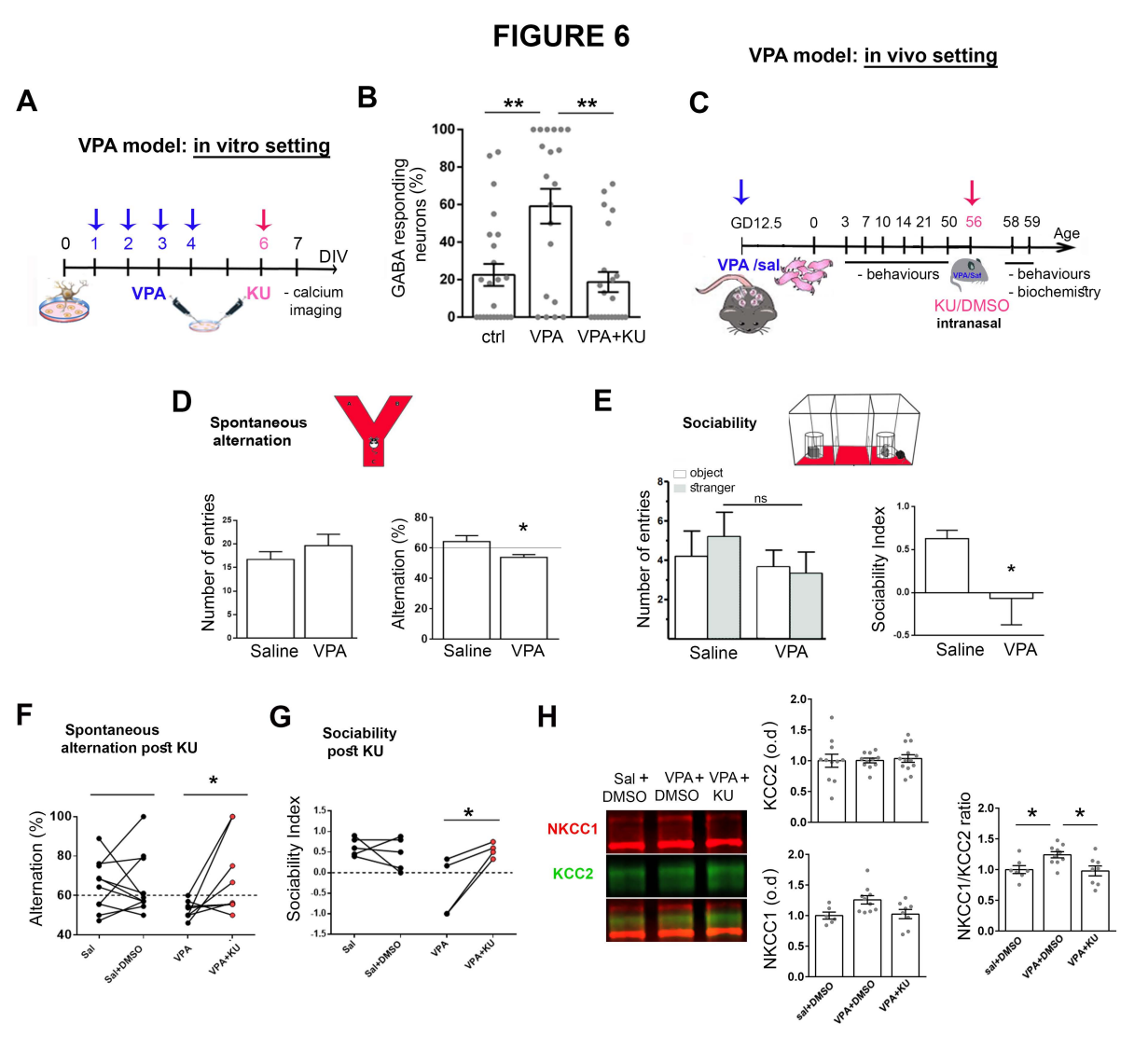
VPA model: in vivo setting
A
VPA model: in vitro setting
0 1 2 3 4 6 7 DIV
VPA
KU
- calcium imaging
B
GABA responding neurons (%)
**
**
ctrl
VPA
VPA+KU
C
GD12.5 0 3 7 10 14 21 50 56 58 59 Age
VPA /sal
- behaviours
- behaviours
- biochemistry
KU/DMSO
intranasal
D
Spontaneous alternation
Number of entries
Saline VPA
Alternation (%)
Saline VPA
E
Sociability
object
stranger
ns
Number of entries
Saline VPA
Sociability Index
Saline VPA
F
Spontaneous alternation post KU
Alternation (%)
Sal
Sal+DMSO
VPA
VPA+KU
G
Sociability post KU
Sociability Index
Sal
Sal+DMSO
VPA
VPA+KU
H
Sal + DMSO
VPA+ DMSO
VPA + KU
NKCC1
KCC2
KCC2 (o.d)
NKCC1 (o.d)
sal+DMSO
VPA+DMSO
VPA+KU
NKCC1/KCC2 ratio
sal+DMSO
VPA+DMSO
VPA+KU

Fig 7. Cartoon of the proposed model: Our model proposes that in WT developing neurons the proper expression and functioning levels of ATM, Mecp2 and Egr4 mediate the right KCC2/NKCC1 amount and thus the correct maturation of GABAergic system. This condition generates the physiological excitatory/inhibitory balance in the network. In *Atm*$^{+/-}$ neurons the higher expression of Mecp2 and Egr4 activity generate increased levels of KCC2 associated to reduced NKCC1 and consequently a premature GABA switch. Based on the trophic GABA action, this mediates a higher inhibition. On the contrary, in a condition of ASD the higher ATM levels associates to a lower Mecp2 expression, reduced KCC2 quantity and increased NKCC1 with a persistent excitatory GABA effect. The transient blockade of ATM kinase action achieved by KU rescues these pathological modifications leading to the normal neuronal firing.

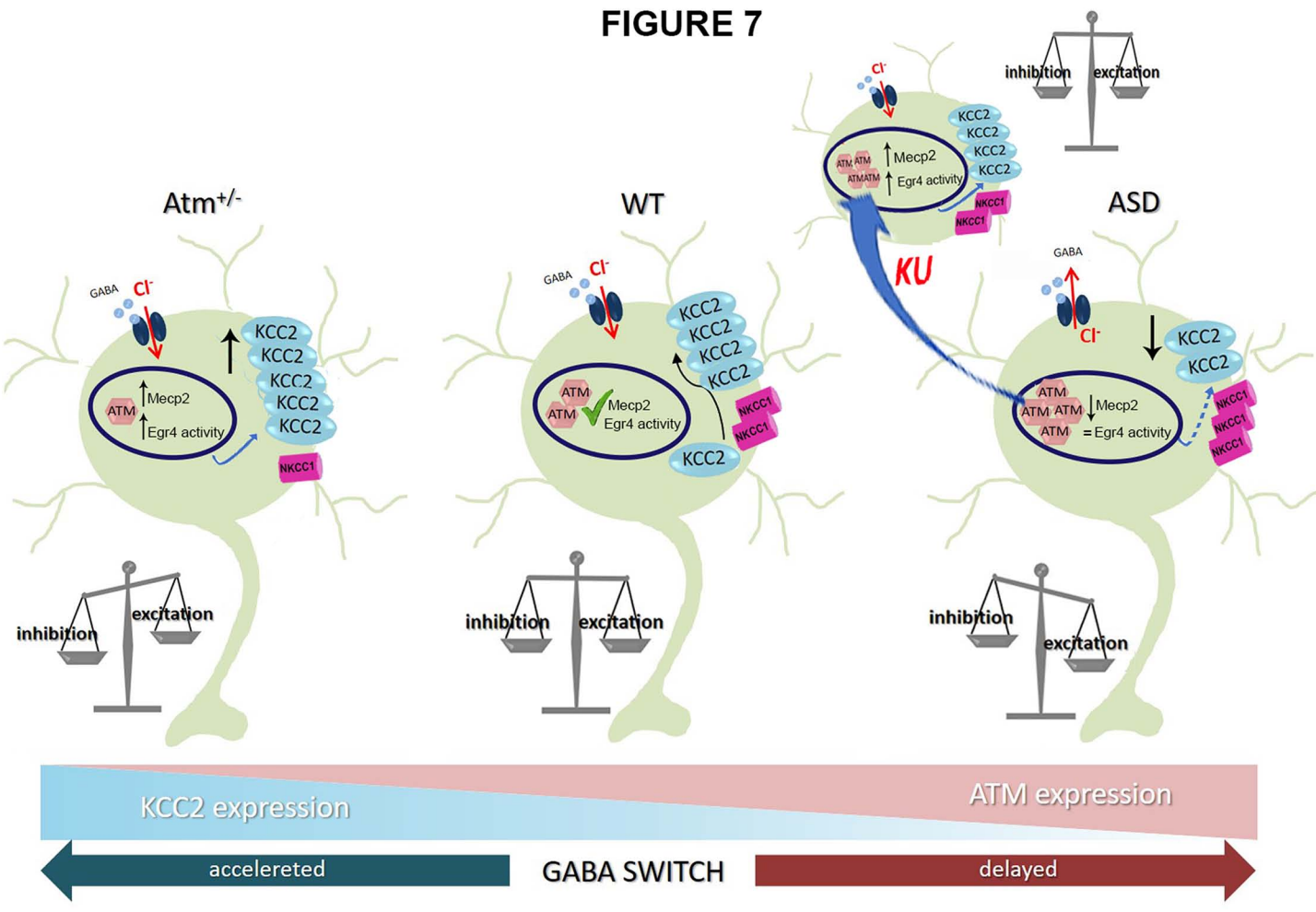

REFERENCES:

1. Corradini, I., et al., *Maternal Immune Activation Delays Excitatory-to-Inhibitory Gamma-Aminobutyric Acid Switch in Offspring.* Biol Psychiatry, 2018. **83**(8): p. 680-691.
2. Deidda, G., et al., *Reversing excitatory GABAAR signaling restores synaptic plasticity and memory in a mouse model of Down syndrome.* Nat Med, 2015. **21**(4): p. 318-26.
3. Leonzino, M., et al., *The Timing of the Excitatory-to-Inhibitory GABA Switch Is Regulated by the Oxytocin Receptor via KCC2.* Cell Rep, 2016. **15**(1): p. 96-103.
4. Silayeva, L., et al., *KCC2 activity is critical in limiting the onset and severity of status epilepticus.* Proc Natl Acad Sci U S A, 2015. **112**(11): p. 3523-8.
5. Han, S., et al., *Autistic-like behaviour in Scn1a+/- mice and rescue by enhanced GABA-mediated neurotransmission.* Nature, 2012. **489**(7416): p. 385-90.
6. Levitt, P., K.L. Eagleson, and E.M. Powell, *Regulation of neocortical interneuron development and the implications for neurodevelopmental disorders.* Trends Neurosci, 2004. **27**(7): p. 400-6.
7. Lewis, D.A., et al., *Cortical parvalbumin interneurons and cognitive dysfunction in schizophrenia.* Trends Neurosci, 2012. **35**(1): p. 57-67.
8. Yizhar, O., et al., *Neocortical excitation/inhibition balance in information processing and social dysfunction.* Nature, 2011. **477**(7363): p. 171-8.
9. Ben-Ari, Y., *Excitatory actions of gaba during development: the nature of the nurture.* Nat Rev Neurosci, 2002. **3**(9): p. 728-39.
10. Leinekugel, X., et al., *GABA is the principal fast-acting excitatory transmitter in the neonatal brain.* Adv Neurol, 1999. **79**: p. 189-201.
11. Leinekugel, X., et al., *Ca2+ oscillations mediated by the synergistic excitatory actions of GABA(A) and NMDA receptors in the neonatal hippocampus.* Neuron, 1997. **18**(2): p. 243-55.
12. Owens, D.F., et al., *Excitatory GABA responses in embryonic and neonatal cortical slices demonstrated by gramicidin perforated-patch recordings and calcium imaging.* J Neurosci, 1996. **16**(20): p. 6414-23.
13. Owens, D.F. and A.R. Kriegstein, *Is there more to GABA than synaptic inhibition?* Nat Rev Neurosci, 2002. **3**(9): p. 715-27.
14. Dammerman, R.S., et al., *An excitatory GABAergic plexus in developing neocortical layer 1.* J Neurophysiol, 2000. **84**(1): p. 428-34.
15. Ohkuma, S., et al., *GABAA receptor stimulation enhances NMDA-induced Ca2+ influx in mouse cerebral cortical neurons in primary culture.* Brain Res Mol Brain Res, 1994. **27**(1): p. 145-51.
16. Sammler, E., S. Titz, and S. Hormuzdi, *Neuronal chloride transport tuning.* Lancet, 2015. **385 Suppl 1**: p. S85.
17. Pizzamiglio, L., et al., *New Role of ATM in Controlling GABAergic Tone During Development.* Cereb Cortex, 2016. **26**(10): p. 3879-88.
18. Li, J., et al., *Cytoplasmic ATM in neurons modulates synaptic function.* Curr Biol, 2009. **19**(24): p. 2091-6.
19. Lim, D.S., et al., *ATM binds to beta-adaptin in cytoplasmic vesicles.* Proc Natl Acad Sci U S A, 1998. **95**(17): p. 10146-51.
20. Guo, Z., et al., *ATM activation by oxidative stress.* Science, 2010. **330**(6003): p. 517-21.
21. Kamsler, A., et al., *Increased oxidative stress in ataxia telangiectasia evidenced by alterations in redox state of brains from Atm-deficient mice.* Cancer Res, 2001. **61**(5): p. 1849-54.
22. Cholewa-Waclaw, J., et al., *The Role of Epigenetic Mechanisms in the Regulation of Gene Expression in the Nervous System.* J Neurosci, 2016. **36**(45): p. 11427-11434.
23. Gomez-Herreros, F., et al., *TDP2 protects transcription from abortive topoisomerase activity and is required for normal neural function.* Nat Genet, 2014. **46**(5): p. 516-21.
24. Lee, Y.H. and G.G. Song, *Genome-wide pathway analysis in attention-deficit/hyperactivity disorder.* Neurol Sci, 2014. **35**(8): p. 1189-96.
25. Lin, P.I., et al., *Runs of homozygosity associated with speech delay in autism in a taiwanese han population: evidence for the recessive model.* PLoS One, 2013. **8**(8): p. e72056.

26. Tang, X., et al., *KCC2 rescues functional deficits in human neurons derived from patients with Rett syndrome.* Proc Natl Acad Sci U S A, 2016. **113**(3): p. 751-6.
27. Banerjee, A., et al., *Jointly reduced inhibition and excitation underlies circuit-wide changes in cortical processing in Rett syndrome.* Proc Natl Acad Sci U S A, 2016. **113**(46): p. E7287-E7296.
28. Duarte, S.T., et al., *Abnormal expression of cerebrospinal fluid cation chloride cotransporters in patients with Rett syndrome.* PLoS One, 2013. **8**(7): p. e68851.
29. Tyzio, R., et al., *Oxytocin-mediated GABA inhibition during delivery attenuates autism pathogenesis in rodent offspring.* Science, 2014. **343**(6171): p. 675-9.
30. Fukuchi, M., et al., *Valproic acid induces up- or down-regulation of gene expression responsible for the neuronal excitation and inhibition in rat cortical neurons through its epigenetic actions.* Neurosci Res, 2009. **65**(1): p. 35-43.
31. Li, Y. and D.Q. Yang, *The ATM inhibitor KU-55933 suppresses cell proliferation and induces apoptosis by blocking Akt in cancer cells with overactivated Akt.* Mol Cancer Ther, 2010. **9**(1): p. 113-25.
32. Batey, M.A., et al., *Preclinical evaluation of a novel ATM inhibitor, KU59403, in vitro and in vivo in p53 functional and dysfunctional models of human cancer.* Mol Cancer Ther, 2013. **12**(6): p. 959-67.
33. Nadkarni, A., et al., *ATM inhibitor KU-55933 increases the TMZ responsiveness of only inherently TMZ sensitive GBM cells.* J Neurooncol, 2012. **110**(3): p. 349-57.
34. Ivanov, V.N., et al., *Inhibition of ataxia telangiectasia mutated kinase activity enhances TRAIL-mediated apoptosis in human melanoma cells.* Cancer Res, 2009. **69**(8): p. 3510-9.
35. Stagni, V., et al., *ATM kinase sustains HER2 tumorigenicity in breast cancer.* Nat Commun, 2015. **6**: p. 6886.
36. Vecchio, D., et al., *Pharmacokinetics, pharmacodynamics and efficacy on pediatric tumors of the glioma radiosensitizer KU60019.* Int J Cancer, 2015. **136**(6): p. 1445-57.
37. Farkas, T., M. Daugaard, and M. Jaattela, *Identification of small molecule inhibitors of phosphatidylinositol 3-kinase and autophagy.* J Biol Chem, 2011. **286**(45): p. 38904-12.
38. Coyne, A.N., et al., *Post-transcriptional Inhibition of Hsc70-4/HSPA8 Expression Leads to Synaptic Vesicle Cycling Defects in Multiple Models of ALS.* Cell Rep, 2017. **21**(1): p. 110-125.
39. Liu, T., C.K. Daniels, and S. Cao, *Comprehensive review on the HSC70 functions, interactions with related molecules and involvement in clinical diseases and therapeutic potential.* Pharmacol Ther, 2012. **136**(3): p. 354-74.
40. Chudotvorova, I., et al., *Early expression of KCC2 in rat hippocampal cultures augments expression of functional GABA synapses.* J Physiol, 2005. **566**(Pt 3): p. 671-9.
41. Wang, Y., et al., *Differential effects of GABA in modulating nociceptive vs. non-nociceptive synapses.* Neuroscience, 2015. **298**: p. 397-409.
42. Sombati, S. and R.J. Delorenzo, *Recurrent spontaneous seizure activity in hippocampal neuronal networks in culture.* J Neurophysiol, 1995. **73**(4): p. 1706-11.
43. Xie, W., et al., *The suppression of epileptiform discharges in cultured hippocampal neurons is regulated via alterations in full-length tropomyosin-related kinase type B receptors signalling activity.* European Journal of Neuroscience, 2014. **40**(3): p. 2564-2575.
44. Logothetis, N.K., *The underpinnings of the BOLD functional magnetic resonance imaging signal.* Journal of Neuroscience, 2003. **23**(10): p. 3963-3971.
45. Uvarov, P., et al., *Upregulation of the neuron-specific K+/Cl- cotransporter expression by transcription factor early growth response 4.* J Neurosci, 2006. **26**(52): p. 13463-73.
46. Ludwig, A., et al., *Early growth response 4 mediates BDNF induction of potassium chloride cotransporter 2 transcription.* J Neurosci, 2011. **31**(2): p. 644-9.
47. Uvarov, P., et al., *Neuronal K+/Cl- co-transporter (KCC2) transgenes lacking neurone restrictive silencer element recapitulate CNS neurone-specific expression and developmental up-regulation of endogenous KCC2 gene.* J Neurochem, 2005. **95**(4): p. 1144-55.
48. Roullet, F.I., et al., *Behavioral and molecular changes in the mouse in response to prenatal exposure to the anti-epileptic drug valproic acid.* Neuroscience, 2010. **170**(2): p. 514-22.
49. Schneider, T. and R. Przewlocki, *Behavioral alterations in rats prenatally exposed to valproic acid: animal model of autism.* Neuropsychopharmacology, 2005. **30**(1): p. 80-9.

50. Silverman, J.L., et al., *Behavioural phenotyping assays for mouse models of autism.* Nat Rev Neurosci, 2010. **11**(7): p. 490-502.
51. Kahle, K.T., et al., *Genetically encoded impairment of neuronal KCC2 cotransporter function in human idiopathic generalized epilepsy.* EMBO Rep, 2014. **15**(7): p. 766-74.
52. Puskarjov, M., et al., *A variant of KCC2 from patients with febrile seizures impairs neuronal Cl- extrusion and dendritic spine formation.* EMBO Rep, 2014. **15**(6): p. 723-9.
53. Fernandes, N.D., Y. Sun, and B.D. Price, *Activation of the kinase activity of ATM by retinoic acid is required for CREB-dependent differentiation of neuroblastoma cells.* J Biol Chem, 2007. **282**(22): p. 16577-84.
54. Chwastek, J., D. Jantas, and W. Lason, *The ATM kinase inhibitor KU-55933 provides neuroprotection against hydrogen peroxide-induced cell damage via a gammaH2AX/p-p53/caspase-3-independent mechanism: Inhibition of calpain and cathepsin D.* Int J Biochem Cell Biol, 2017. **87**: p. 38-53.
55. Madabhushi, R., et al., *Activity-Induced DNA Breaks Govern the Expression of Neuronal Early-Response Genes.* Cell, 2015. **161**(7): p. 1592-605.
56. Suberbielle, E., et al., *Physiologic brain activity causes DNA double-strand breaks in neurons, with exacerbation by amyloid-beta.* Nat Neurosci, 2013. **16**(5): p. 613-21.
57. West, A.E. and M.E. Greenberg, *Neuronal activity-regulated gene transcription in synapse development and cognitive function.* Cold Spring Harb Perspect Biol, 2011. **3**(6).
58. Knobloch, H.S., et al., *Evoked axonal oxytocin release in the central amygdala attenuates fear response.* Neuron, 2012. **73**(3): p. 553-66.
59. Curia, G., et al., *Downregulation of tonic GABAergic inhibition in a mouse model of fragile X syndrome.* Cereb Cortex, 2009. **19**(7): p. 1515-20.
60. Akbarian, S., et al., *GABAA receptor subunit gene expression in human prefrontal cortex: comparison of schizophrenics and controls.* Cereb Cortex, 1995. **5**(6): p. 550-60.
61. Impagnatiello, F., et al., *A decrease of reelin expression as a putative vulnerability factor in schizophrenia.* Proc Natl Acad Sci U S A, 1998. **95**(26): p. 15718-23.
62. Calfa, G., et al., *Excitation/inhibition imbalance and impaired synaptic inhibition in hippocampal area CA3 of Mecp2 knockout mice.* Hippocampus, 2015. **25**(2): p. 159-68.
63. Li, W., X. Xu, and L. Pozzo-Miller, *Excitatory synapses are stronger in the hippocampus of Rett syndrome mice due to altered synaptic trafficking of AMPA-type glutamate receptors.* Proc Natl Acad Sci U S A, 2016. **113**(11): p. E1575-84.
64. Lu, X.H., et al., *Targeting ATM ameliorates mutant Huntingtin toxicity in cell and animal models of Huntington's disease.* Sci Transl Med, 2014. **6**(268): p. 268ra178.
65. Dargaei, Z., et al., *Restoring GABAergic inhibition rescues memory deficits in a Huntington's disease mouse model.* Proc Natl Acad Sci U S A, 2018. **115**(7): p. E1618-E1626.
66. Antonucci, F., et al., *Cracking down on inhibition: selective removal of GABAergic interneurons from hippocampal networks.* J Neurosci, 2012. **32**(6): p. 1989-2001.
67. Laird, P.W., et al., *Simplified Mammalian DNA Isolation Procedure.* Nucleic Acids Research, 1991. **19**(15): p. 4293-4293.
68. Bedogni, F., et al., *Defects During Mecp2 Null Embryonic Cortex Development Precede the Onset of Overt Neurological Symptoms.* Cereb Cortex, 2016. **26**(6): p. 2517-2529.
69. Murru, L., et al., *Pharmacological Modulation of AMPAR Rescues Intellectual Disability-Like Phenotype in Tm4sf2-/y Mice.* Cereb Cortex, 2017. **27**(11): p. 5369-5384.
70. Tomasoni, R., et al., *Lack of IL-1R8 in neurons causes hyperactivation of IL-1 receptor pathway and induces MECP2-dependent synaptic defects.* Elife, 2017. **6**.
71. Nicolini, C. and M. Fahnestock, *The valproic acid-induced rodent model of autism.* Exp Neurol, 2018. **299**(Pt A): p. 217-227.
72. Rodier, P.M., et al., *Embryological origin for autism: developmental anomalies of the cranial nerve motor nuclei.* J Comp Neurol, 1996. **370**(2): p. 247-61.
73. Moldrich, R.X., et al., *Inhibition of histone deacetylase in utero causes sociability deficits in postnatal mice.* Behav Brain Res, 2013. **257**: p. 253-64.

74. Begenisic, T., et al., *Fluoxetine in adulthood normalizes GABA release and rescues hippocampal synaptic plasticity and spatial memory in a mouse model of Down syndrome.* Neurobiol Dis, 2014. **63**: p. 12-9.
75. Sala, M., et al., *Pharmacologic rescue of impaired cognitive flexibility, social deficits, increased aggression, and seizure susceptibility in oxytocin receptor null mice: a neurobehavioral model of autism.* Biol Psychiatry, 2011. **69**(9): p. 875-82.